

Chlorine Adsorption on Graphene: Chlorographene

H. Şahin^{1,2,*} and S. Ciraci^{1,2,3,†}

¹*UNAM-National Nanotechnology Research Center, Bilkent University, 06800 Ankara, Turkey*

²*Institute of Materials Science and Nanotechnology, Bilkent University, 06800 Ankara, Turkey*

³*Department of Physics, Bilkent University, 06800 Ankara, Turkey*

(Dated: November 27, 2024)

We perform first-principles structure optimization, phonon frequency and finite temperature molecular dynamics calculations based on density functional theory to study the interaction of chlorine atoms with graphene predicting the existence of possible chlorinated graphene derivatives. The bonding of a single chlorine atom is ionic through the transfer of charge from graphene to chlorine adatom and induces negligible local distortion in the underlying planar graphene. Different from hydrogen and fluorine adatoms, the migration of a single chlorine adatom on the surface of perfect graphene takes place almost without barrier. However, the decoration of one surface of graphene with Cl adatoms leading to various conformations cannot sustain due to strong Cl-Cl interaction resulting in the desorption through the formation of Cl₂ molecules. On the contrary, the fully chlorinated graphene, chlorographene CCl, where single chlorine atoms are bonded alternately to each carbon atom from different sides of graphene with *sp*³-type covalent bonds, is buckled. We found that this structure is stable and is a direct band gap semiconductor, whose band gap can be tuned by applied uniform strain. Calculated phonon dispersion relation and four Raman-active modes of chlorographene are discussed.

PACS numbers: 73.22.Pr, 63.22.Rc, 61.48.Gh, 71.15.Mb

I. INTRODUCTION

The synthesis of graphene^{1,2} has led to intense research activity in the field of graphene-based nanoscale devices. Although graphene is one of the most mechanically strong material having a wide range of extraordinary properties,^{1–5} practical device applications are limited by its metallic behavior and sensitivity to surface adsorbates.

Efforts to synthesize chemically modified graphene composites with tailored electronic, optical, and chemical properties have presented new directions in graphene research. In particular, band gap engineering of graphene through chemical modification, such as oxygenation,^{6–11} and hydrogenation^{12–17} is appealing for electronic applications, since the scalable fabrication of graphene-based devices without disturbing the strong honeycomb lattice has become possible. However, due to the complex atomic structure of grapheneoxides⁷ (GOs) and thermal instabilities of hydrogenated graphenes (CHs) even at low temperatures,^{12–14} search for the novel graphene-based materials is still continuing.

Over the past three years experimental^{18–21} and theoretical^{22,23} studies have demonstrated that chemical conversion of graphene to fluorographene (CF) is possible. In addition to early studies on the atomic composition and band structure of fluorocarbon materials,^{24,25} it was reported that the monolayer CF has quite different vibrational spectra and Raman characteristics as compared to hydrogenated graphene analogues.²² We also investigated the electronic and elastic properties of possible fluorinated graphene materials and attempted to clarify the discrepancy between theoretical and experimental results.²³ Easy synthesis, high-quality insulating

behavior and extraordinary mechanical strength of fluorographene (CF) have inspired intense research on other halogen decorated graphene derivatives.

In addition to three known derivatives of graphene: GO, CH and CF, the successful synthesis of chlorinated graphene was also achieved very recently.²⁶ It is experimentally demonstrated that nondestructive and patternable conversion of graphene is possible by using various photochemical chlorination techniques.^{26–28} While the research on chlorine-graphene interaction is rapidly growing,^{26–36} comprehensive research on the stability of various chlorinated graphene structures and their resulting properties are sparse.

In this paper we present a detailed analysis of the interaction between chlorine atom and graphene leading to the chlorination of graphene. Although the possibility of covering graphene surfaces with chlorine atoms has been reported, analyses of structural stability, electronic and magnetic properties as a function of Cl coverage are lacking. Our main motivation is to reveal which conformations of chlorinated graphene are stable and how these conformations modify the properties of graphene. To this end we investigated the chlorination of graphene starting from single Cl adsorption to full coverage leading to chlorographene, namely CCl. At low coverage with diminishing Cl-Cl coupling, the binding of Cl to graphene is significant, but adsorbed Cl atoms migrate on the surface of graphene almost without an energy barrier. We found that the nonbonding chair conformation of chlorographene^{30,31} (CCl) consisting of a planar graphene sandwiched between widely spaced two planar Cl layers is unstable. On the other hand, the covalently bonded chair conformation of the chlorographene (CCl) is found to be stable at T=0 K and possibly at room

temperature. This latter conformation consists of buckled graphene sandwiched between two planar Cl layers and is a nonmagnetic semiconductor with 1.2 eV direct band gap. Our results reconcile the discrepancy between the experimental study²⁶ obtaining semiconducting properties upon the chlorination of graphene and theoretical studies predicting metallic state.^{30,31}

II. COMPUTATIONAL METHODOLOGY

To investigate mechanical, electronic magnetic properties of chlorinated graphene we carried out first-principles density functional theory (DFT) calculations within the local density approximation (LDA)³⁸ using projector augmented wave (PAW) potentials.³⁷ All results discussed in the text are obtained using LDA. To compare with the LDA results of specific systems, we also performed calculations using Generalized Gradient Approximation³⁹(GGA) together with van der Waals (vdW) correction, (GGA+vdW).⁴⁰ In our earlier tests LDA yielded interlayer spacings of layered materials and other structural parameters in agreement with experimental data, as well as with those obtained by using GGA+vdW. In the vdW corrections of the later method, DFT description is restricted to shorter correlation length scales, but for the medium and large inter-atomic distances the damped C_6r^{-6} term is used. The systems, whose numerical values are also obtained by using GGA+vdW are indicated. Numerical calculations are performed using VASP.⁴¹ Kinetic energy cutoff, $E_{cut} = \hbar^2|\mathbf{k} + \mathbf{G}|^2/2m$, for plane-wave basis set is taken as 500 eV. A vacuum spacing of at least 15 Å is placed between adjacent layers to hinder the layer-layer interactions. The convergence criterion of self consistent calculations for ionic relaxations is 10^{-5} eV between two consecutive steps. Structural optimizations were performed using a conjugate gradient algorithm with a convergence criterion of 10^{-4} eV/Å. Pressures on the lattice unit cell are decreased to values less than 1.0 kBar. The adsorption of a single Cl atom to graphene surface is treated using the supercell geometry, where single Cl is adsorbed to each (4x4) supercell. In the self-consistent potential and total energy calculations using a (4x4) supercell of chlorographene, a set of (13x13x1) \mathbf{k} -point sampling is used for Brillouin zone (BZ) integration. The sampling of BZ is then scaled according to the sizes of the supercells used for other systems. Ground state electronic structures are calculated by applying a dipole correction to eliminate the artificial electrostatic field between periodic supercells. For the charge transfer analysis, the effective charge on atoms are obtained by Bader method.⁴²

The stabilities of structures having various Cl coverage are examined by the calculation of phonon frequencies for \mathbf{q} -wave vectors over BZ by using both small displacement method (SDM)⁴³ and density functional perturbation theory (DFPT).⁴⁴ We used 196-atom supercell of chlorographene, \mathbf{q} -point sampling grid of 3x3x1 and

0.01 Å displacements in calculations using SDM. DFPT part of the phonon calculations were performed by using 6x6x1 grid of \mathbf{q} -points for chlorographene unitcell. A given structure is considered to be stable, if vibration frequencies are positive for all \mathbf{q} -points in BZ.

The energy band gap, which is usually underestimated by DFT, is corrected by frequency-dependent GW_0 calculations.⁴⁵ In GW_0 corrections screened Coulomb potential W , is kept fixed to initial DFT value W_0 and Green's function G , is iterated four times. Finally, the band gap of CCl is calculated by using (12x12x1) \mathbf{k} -points in BZ, 20 Å vacuum spacing, default cut-off potential for GW_0 , 160 bands and 64 grid points.

The binding energy of a single adatom X to the graphene supercell (i.e. X=H hydrogenation; X=F fluorination; X=Cl chlorination) is calculated according to the expression, $E_b = E_T[Gr] + E_T[X] - E_T[Gr + X]$, in terms of the ground state total energies⁴⁶ of bare graphene $E_T[Gr]$, free X atom $E_T[X]$, and X adsorbed to graphene $E_T[Gr + X]$. Accordingly, $E_b > 0$ indicates a bound state. Similarly, the formation energy of a single adatom adsorbed to graphene supercell relative to X_2 molecule is defined as $E_f = E_T[X_2]/2 + E_T[Gr] - E_T[Gr + X]$, where $E_T[X_2]$ is the ground state total energy⁴⁶ of X_2 molecule. For an exothermic process $E_f > 0$. The cohesive energy of graphene fully covered with X, CX relative to free C and X atoms is defined as $E_{coh} = 2E_T[X] + 2E_T[C] - E_T[CX]$, where $E_T[CX]$ is the total ground state energy (per unit cell) of CX. By definition $E_{coh} > 0$ indicates binding relative to individual constituent atoms.

III. ADSORPTION OF SINGLE CHLORINE

Understanding of the adsorption process of a single Cl adatom on graphene is essential for the investigation of its chlorinated derivatives. The Cl-Cl coupling between adsorbed Cl atoms is crucial. Here, the Cl coverage is defined as the ratio of the number of Cl atoms N_{Cl} to the number of carbon atoms N_C in a supercell; namely $\Theta = N_{Cl}/N_C$. A single Cl atom adsorbed to graphene is represented by a system where a Cl atom is adsorbed to each (4x4) supercell. This actually corresponds to a uniform coverage of $\Theta=0.03125$. Based on the analysis discussed in the next section we found the size of (4x4) supercell is sufficient to neglect the Cl-Cl coupling. Even if the Pauling scale of electronegativity of specific atoms alone cannot provide criteria for the character and strength of the bonds between those atoms, it usually indicates useful correlations. For example, according to the Pauling scale of electronegativity (H: 2.20, C: 2.55, Cl: 3.16 and F: 3.98) the binding of Cl atoms to graphene can be expected to be stronger than that of hydrogen adatoms (0.98 eV) and weaker than the fluorine adatoms (2.71 eV). Three different adsorption sites can be foreseen for the adsorption of Cl on graphene as described in Fig. 1(a). These are the hollow (H) site above the cen-

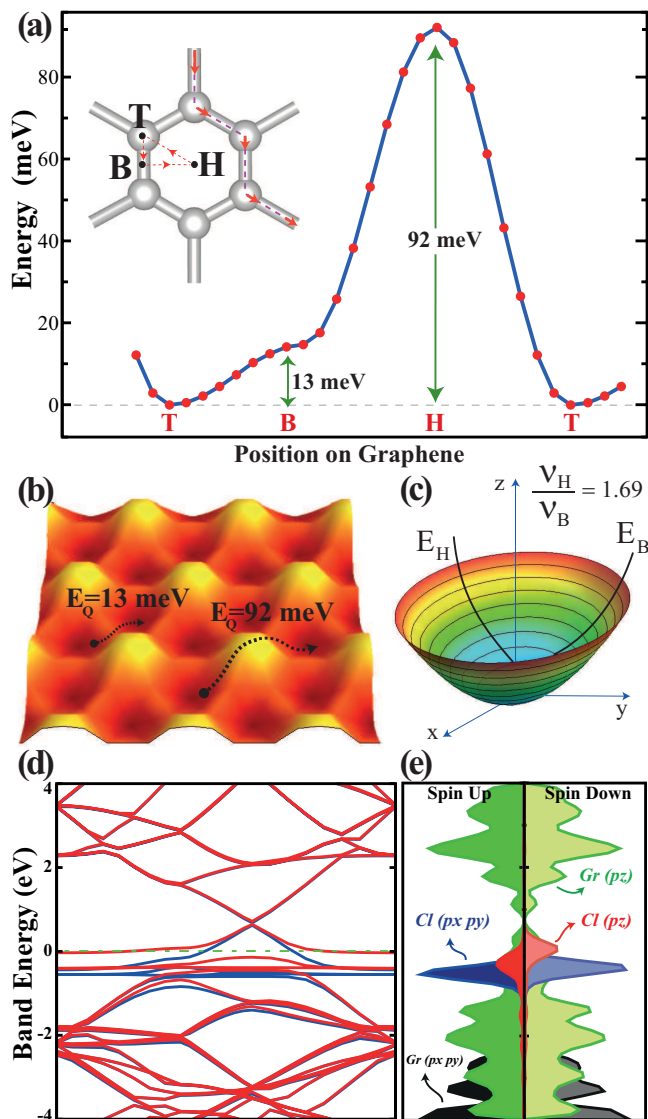


FIG. 1: (Color online) (a) Variation of energy for a single Cl adatom along the symmetry direction of a hexagon. Zero of energy is set to the energy of T-site. The diffusion path with the lowest energy barrier of $Q=13$ meV between two adjacent T-sites are marked with thick red/ dashed lines. (b) Energy landscape of a single Cl adatom adsorbed to graphene. Dark (light) colors represents the top (hollow) sites. (c) Potential energy contour plots (paraboloid) of Cl adatom around the T-site. The jump frequency of Cl atom ν , for different directions are calculated from this paraboloid. (d) Band structure of a single Cl adsorbed to each (4×4) supercell of graphene and corresponding total (TDOS) and orbital decomposed (PDOS) densities of states. The zero of band energy is set to the Fermi level.

ter of hexagon, the top (T) site on top of C atoms, the bridge (B) site above the middle of C-C bonds. Among these sites, the strongest binding of single Cl to graphene is attained at T-site with a binding energy of $E_b=1.10$ eV (E_b calculated using GGA+vdW 1.16 eV). Earlier studies dealing with graphene-Cl interaction calculated the

binding energies of Cl adatom ranging 1.05 eV³⁵ using (4×4) supercell and 0.8 eV.²⁹ Using a methodology similar to that used in the present work the binding energy of Cl adatom is calculated to be 1.13 eV.³⁶ Applying correction based on hybrid functionals⁴⁷ and hence performing GGA+HSE06 calculations we found the binding energy of Cl as 0.7 eV.

The variation of the total energy of an adsorbed Cl atom at the symmetry points and along the symmetry (T-B-H-T) directions of a hexagon in the (4×4) supercell is shown in Fig. 1 (a). At each point on the energy curve, x - and y -positions of adsorbed Cl atom are fixed, its z -height, as well as positions of all C atoms in the (4×4) supercell are optimized by minimizing total energy and atomic forces. Using this energy curve we reveal the energy barriers to be overcome by the adsorbate migrating or diffusing on the surface of graphene. The minimum energy barrier occurs at the B-site between two adjacent T-site. The relevant energy barriers are shown on the calculated energy landscaping presented in Fig. 1 (b). This analysis suggests that a diffusing Cl atom can take a path of minimum energy barrier following the edges of hexagon from T-site to T-site through the barrier of $Q=13$ meV at B-site. This energy barrier is in fair agreement calculated by Wehling et al.²⁹ We note that this barrier is very low and allows Cl atom to migrate on the surface of graphene as if it rolls along the edges of hexagon. This is a remarkable situation, where the migration or diffusion of Cl occurs with almost no barrier, but it remains bound to the surface. This property of Cl adatom on graphene heralds a number of possible applications, such as superlow sliding friction, sensors and devices for energy harvesting.³⁴ The binding energy of an isolated Cl_2 molecule is calculated to be 3.58 eV,⁴⁸ leading to negative formation energy $E_f < 0$. Then the adsorption of chlorine on graphene is an endothermic process and hence it can be achieved by, for example, the assistance of light absorption.²⁶

In Fig. 1 (c) the energy plot $E_T(x, y)$ (or energy paraboloid) of Cl adatom displacing from its equilibrium position at T-site is deduced approximately from the energy landscaping shown in Fig. 1 (b). When displaced along T-H and T-B directions, the Cl adatom undergoes different energy variations. Using this energy plot and the model related with simple harmonic oscillator we estimate the values of jump frequencies of adatom towards H- and B-sites to be $\nu_{T \rightarrow B} \sim 0.97$ THz and $\nu_{T \rightarrow H} \sim 1.68$ THz, respectively. The diffusion constant at a given temperature can be obtained from a simple expression,⁴⁹ $D = \nu a^2 \exp(-Q/k_B T)$ in terms of energy barrier Q , lattice constant a and the characteristic jump frequency ν . Using these values the diffusion constant at $T=300$ K is calculated for the barrier $Q=13$ meV to be $D=3.57$ cm^2/s . This indicates that Cl adatom migrates readily over the graphene layer.

The length of Cl-C bond is found to be $d_{\text{Cl-C}}=2.54$ Å. This value is larger than the bond length calculated from the sum of covalent radii of Cl and C atoms,⁴⁹ namely

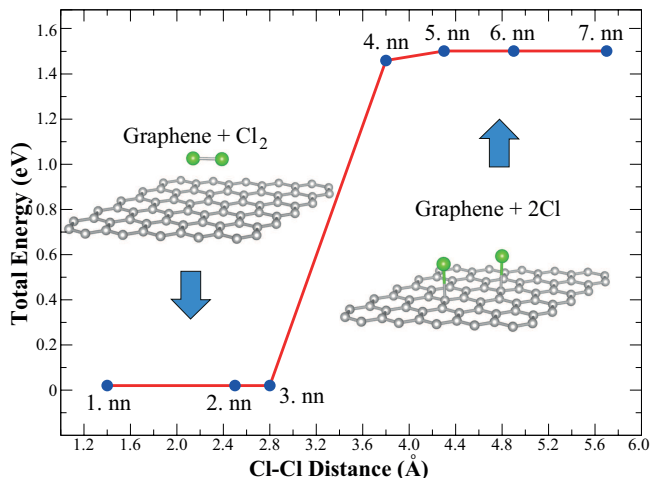


FIG. 2: (Color online) The interaction energy between two Cl atoms adsorbed to the same side of a (6x6) supercell of graphene. The zero of energy is set to the energy of Cl₂ plus graphene. nn denotes the nearest neighbor in graphene lattice

$r_{Cl} + r_C = 1.75\text{\AA}$, as well as the bond lengths of CCl₄ (1.77 Å). This situation indicates that the character of this bond is rather different from C-Cl covalent bond in CCl₄. When single Cl is adsorbed to graphene, 0.44 e is transferred from graphene to Cl adatom according to Bader analysis.⁴² The calculated charge transfer, as well as the analysis of charge density distribution indicates an ionic character for the Cl-C bond.³⁶ The negative charge on Cl induces a dipole moment of $\mathbf{p}=0.67 e\text{-\AA}$ when a single Cl atom is adsorbed to each (4x4) supercell of graphene.⁵⁰ Consequently, the work function of bare graphene which is 4.49 eV increases to 6.53 eV upon Cl adsorption. This the energy required to remove an electron from the Fermi level to the vacuum energy at the side where Cl atoms are adsorbed. Incidentally, while the atomic configuration of graphene beneath Cl adatom is rather flat, H and F adatoms on graphene impose buckling resulting in a covalent character.^{14,23} As we will discuss in the next section, charge transfer from C to Cl and hence the character of the bonding in two sided adsorption is dramatically different.

While single Cl adatom on the surface of graphene can be viewed as an impurity leading to localized (or resonance) states, our model representing the adsorption using a (4x4) supercell gives rise to an energy band structure, where dispersion of bands related with adsorbate can be taken as the measure of adsorbate-adsorbate coupling. The band structure of a single Cl adsorbed to each (4x4) supercell of graphene presented in Fig. 1 (d) has filled chlorine states appearing as flat bands. In view of the negligible dispersions of these bands associated with Cl and the analysis of the bands corresponding to (5x5) and (6x6) supercells in the following section we concluded that a Cl adsorbed to each (4x4) supercell can mimic successfully the single, *i.e.* isolated Cl adsorbed to graphene surface. Because of 7 valence electrons and hence a sin-

gle unfilled 3p orbital occurring below the Fermi level E_F of bare graphene, Cl adsorbed graphene is metalized and becomes magnetic with $\mu=0.56 \mu_B$ due to broken spin degeneracy. The linearly crossing bands of bare graphene is raised above E_F . The orbital decomposed density of states in Fig. 1 (e) show that the flat bands below E_F are derived mainly from Cl-3p_x and Cl-3p_y orbitals.

IV. COVERAGE OF GRAPHENE BY CHLORINE ADATOMS

The interaction between two adsorbed Cl as a function of their separation is important to understand the coverage dependent properties and stability of Cl covered graphene. To this end we consider two Cl atoms adsorbed to the (6x6) supercell of graphene and calculate the total energies as a function of the separation between them. Chlorine atoms are placed at specific adsorption sites by fixing their x - and y -coordinates, but their z -coordinates, as well as the positions of other C atoms in the supercell are relaxed. In Fig. 2 we show how the Cl-Cl interaction changes with their separation. The Cl-Cl coupling is practically negligible when their separation greater or equal to 3.6 Å corresponding to fourth nearest neighbor. For smaller separations corresponding to third nearest neighbor separation of graphene with the threshold distance, they form Cl₂ molecule and desorb from graphene surface, since Cl-Cl interaction energy becomes stronger than the sum of the binding energies of two Cl atoms to graphene (2.20 eV). Accordingly, the gain of energy through the formation of Cl₂ is 1.26 eV per molecule. This explains also why chlorination of graphene is endothermic. There is a weak vdW interaction between bare graphene and Cl₂ molecule. The maximum interaction of 144 meV occurs when the molecule is parallel to a C-C bond and 3 Å above it.

Next we examine how the electronic structure changes with one sided uniform coverage. In Fig. 3 we show the band structures calculated for single Cl atom adsorbed to ($n \times n$) supercell for $n=2,3,5$ and 6. Here $n=2$ and $n=3$ correspond to $\Theta=0.125$ and 0.056. The phonon calculations for these two coverage values are found stable, since the frequencies of phonon modes are positive for any \mathbf{k} -point in BZ. The smallest separation between Cl atoms is larger than the threshold distance of 2.8 Å (*i.e.* the third nearest neighbor distance) even for $\Theta=0.125$. We see that with increasing Θ the dispersion of Cl bands increases slightly and the linearly crossing bands start to split. The magnetic moment also increases with coverage, since the splitting of spin-up and spin-down bands increases. We found $\mu=0.64 \mu_B$ and $\mu=0.56 \mu_B$ for $\Theta=0.0555$ (or $n=3$) and $\Theta=0.020$ (or $n=5$), respectively. On the other hand, a single Cl adsorption to each (1x1) unit cell of graphene (which corresponds to $\Theta=0.5$) is unstable due to Cl-Cl distance smaller than 2.8 Å. Since the uniformly chlorinated graphene is found to be metallic for any coverage studied here, the experimental studies measuring a band

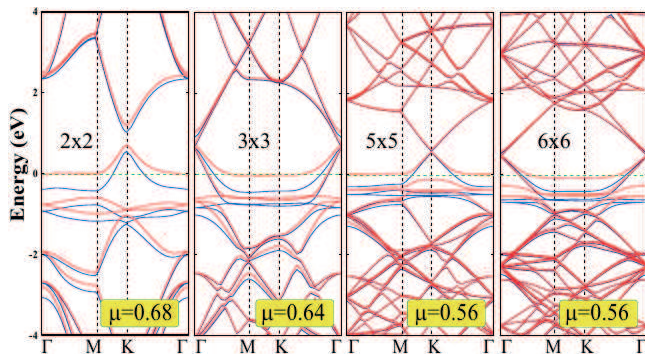


FIG. 3: (Color online) Energy band structure of a single Cl atom adsorbed to each $(n \times n)$ supercell of graphene for $n=2,3,5$ and 6 , which correspond to the one-sided uniform coverage $\Theta = 1/2n^2$. For $n \geq 2$ the distance between nearest Cl adatoms is larger than the threshold distance described in Fig. 2. Whereas stable Cl coverage with $n = 1$ (or $\Theta=0.5$) cannot be achieved due to the strong Cl-Cl coupling. The units of magnetic moments μ is Bohr magneton per $(n \times n)$ supercell. The zero of energy is set at the Fermi level, E_F .

gap of ~ 0.05 eV should correspond to two sided coverage.

To understand the formation of chlorinated domains on graphene, and hence to analyze the kinetics of Cl coverage, we next examine the adsorption of second Cl atom at different sites at the close proximity of the first one in (4×4) supercell. When a Cl is placed on top of a carbon atom, second Cl can be adsorbed on six relevant sites on the hexagonal carbon ring as shown in Fig. 4 (a).

Among the various possible cases, the ortho top-bottom arrangement is the most favorable one. While adsorption of a single Cl atom yields 0.05 \AA buckling of graphene lattice, adjacent C atoms forming C-Cl bonds in ortho top-bottom configuration are buckled by 0.46 \AA . In Fig. 4(b) the contour plots of total charge density on the planes passing through the bonds clearly explain the ionic character of C-Cl bond of a single Cl adatom. In the case of ortho top-bottom the bonding between Cl adatom and C atom of graphene has sp^3 -type covalent character. While the charge density between Cl and C atoms is very low in the ionic case, the bond charge is enhanced in the covalent C-Cl bond. The binding energy of covalent bond is stronger ($E_b=1.53$ eV) and consequently its length is shorter ($d=1.90 \text{ \AA}$, which is comparable with the empirical covalent radii of the C-Cl bond or the bond length $d_{C-Cl}=1.77 \text{ \AA}$ of CCl_4 molecule). The binding energies per bond in the case of meta and para top-bottom configurations are $E_b=1.10$ eV and $E_b=1.31$ eV, respectively. In spite of the fact that the ortho top-bottom configuration is 0.52 eV less energetic than the formation of Cl_2 molecule, it can be stable since the formation of Cl_2 molecule from two Cl atoms at different sides are hindered. In para and meta top-bottom structures, the binding energies of two bonds are further lowered from the formation energy of Cl_2 molecule.

The situation is however dramatically different for one sided (top-top) configurations presented in the second

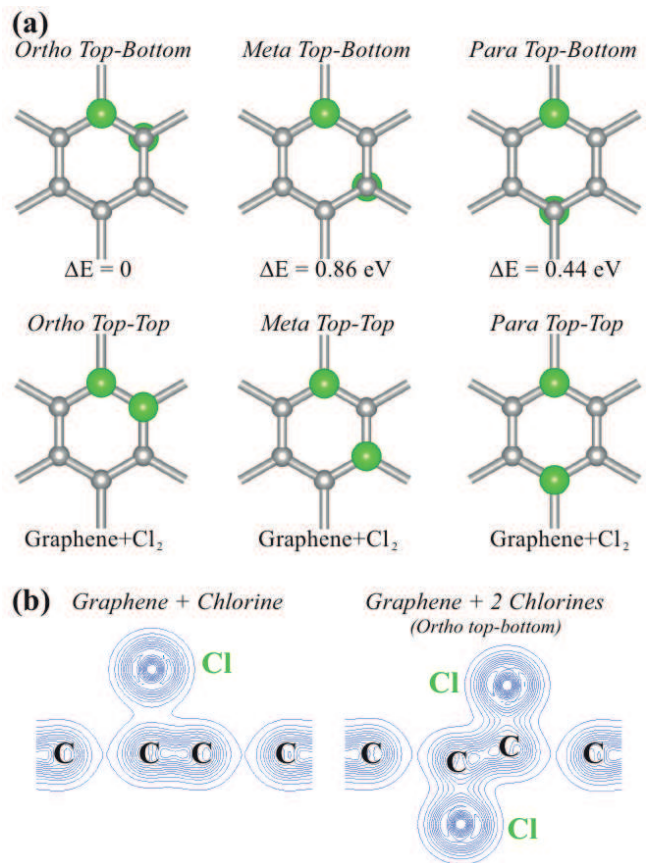


FIG. 4: (Color online) (a) The atomic structure two Cl atoms adsorbed to a (4×4) supercell of graphene. In three different configuration illustrated by top panels, namely ortho top-bottom, para top-bottom and meta top-bottom, two adsorbed Cl atoms are stable. ΔE indicates their energies relative to the total energy of the ortho top-bottom configuration. Double sided adsorption imposes a local buckling in planar graphene. Three one-sided configurations, ortho top-top, para top-top and meta top-top are not allowed; Cl atoms cannot be bound to graphene, they rather form Cl_2 molecule. Large green and small gray balls represent Cl and C atoms, respectively. (b) Contour plots of the total charge density of a single Cl-C bond and two Cl-C bonds in ortho top-bottom configuration. Contours spacings between $0.025 e/\text{\AA}^3$ and $1.0 e/\text{\AA}^3$ are $0.025 e/\text{\AA}^3$.

row of Fig. 4 (a). For these three one-sided configuration, namely ortho, para and meta top-top configurations the Cl-Cl distances are within the third nearest neighbors. Owing to the strong Cl-Cl coupling, the formation of Cl_2 molecule is energetically favored. Accordingly, unlike the half fluorinated graphene²³ (C_2F), one-sided densely chlorinated graphene with the coverage $\Theta=0.5$, namely C_2Cl , cannot be realized.

We now concentrate on the chemical conversion of graphene to a fully chlorinated graphene structure ($\Theta=1.0$), called chlorographene. In addition to well-known boat, chair and nonbonding chair conformations one can also consider zigzag and armchair stoichiomet-

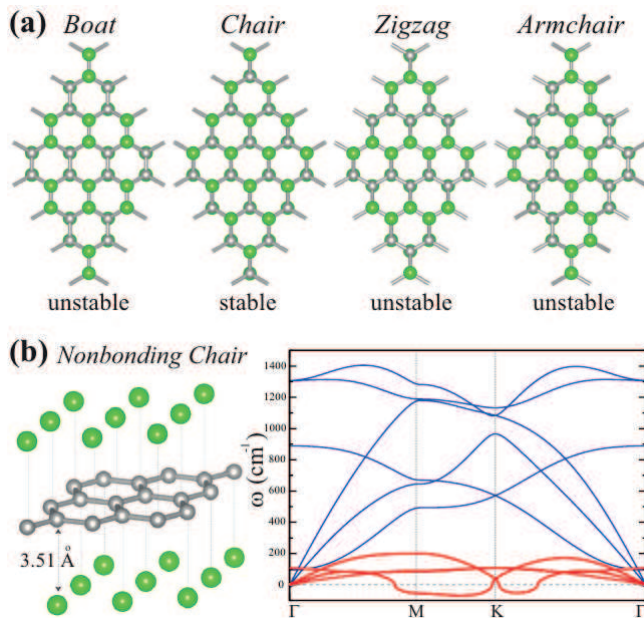


FIG. 5: (Color online) (a) Top view of atomic structures of boat, chair (*i.e.* covalently bonded and buckled graphene layer is sandwiched between two planar Cl layers), zigzag and armchair conformations. Green and small grey balls represent Cl and C atoms, respectively. (b) Side view of nonbonding chair conformation consisting of one planar graphene layer sandwiched by two planar Cl layers and its calculated phonon dispersion curves. Low frequency phonon modes shown by red lines are related to adsorbed Cl atoms. These modes have imaginary frequencies and hence they are unstable.

ric chlorographene configurations shown in Fig. 5. Here, boat, chair, nonbonding chair and zigzag conformations are treated using (2x2) supercell; a (4x4) supercell is required for the armchair conformations. As a consequence of the strong Cl-Cl interaction, boat, zigzag and armchair configurations of Cl atoms cannot remain stable on graphene.

Here the nonbonding chair conformations in Fig. 5 (b) consists of a planar graphene layer sandwiched between two Cl layers deserves a detailed discussion. In this conformation Cl atoms are placed to the alternating T-sites at both sides of graphene. Earlier theoretical studies^{30,31} have predicted that this metallic structure has highest cohesive energy among conformations described in Fig. 5. Present calculations predict $E_T=23.35$ eV/per primitive cell and cohesive energy $E_{coh}=2.79$ eV/ per primitive cell. Even if the structure optimization using conjugate gradient method performed in the (1x1) hexagonal unit cell finds the nonbonding chair structure stable, we carried out an extensive analysis of this conformation. We found that the attractive interaction between each Cl layer and underlying graphene is rather small (50 meV per unit cell) in spite of the fact that graphene lattice expanded by 2.8% and the system attained a total energy ~ 3.31 eV higher than that of graphene. The weak interaction between Cl and C atoms explains why the distance from

Cl layer to graphene is large (3.51 Å). This large distance and minute charge transfer from carbon to Cl atom can be contrasted with the C-Cl distance (2.54 Å) and the transfer of 0.44 electrons from C to Cl of the ionic bond of single Cl atom adsorbed to graphene as discussed in Sec. III. This paradoxical situation occurred due to the strong intra-layer coupling among Cl atoms in both Cl-layers at both sides of graphene. In fact, the binding energy of Cl atoms of a single Cl layer having the same atomic configuration as the Cl layers of nonbonding chair conformation is found to be 1.41 eV per Cl atom. It appears that high cohesive energy of nonbonding chair conformation relative to free graphene and free Cl atoms is attained mainly by the cohesion between Cl atoms, but not by the interaction between Cl and carbon atoms. In addition, GGA+vdW calculations performed for nonbonding conformation resulted with optimized structure close to that obtained by using LDA.

Under these paradoxical situations we further examined the stability of the metallic nonbonding chair conformer by carrying out ab-initio calculations of phonon frequencies in the BZ. As seen in Fig. 5 (b), the calculated phonon branches, which are associated with Cl in-plane and out-of-plane modes and hence are practically isolated from graphene modes and hence are imaginary frequencies near *M*- and *K*-high symmetry points. This clearly indicates that nonbonding chair structure is unstable at $T=0$ K. In fact, a minute displacements or perturbation of atoms in Cl plane is resulted in the breakdown of Cl-layers, if nonbonding chair structure is treated using a (4x4) supercell. It appears that structure optimization in earlier studies^{30,31} carried out in a single cell has limited the degree of freedom of Cl atoms preventing them from reconstructions involving large displacements or from forming molecules. Accordingly, the stability imposed by the structure optimization using primitive cell was unrealistic. Even though the nonbonding chair conformation has the lowest energy among other conformers including (covalently bonded) chair structure in Fig. 5, it corresponds either to a very shallow local minimum or to a saddle point for specific directions of atomic displacements in Born-Oppenheimer surface.

V. STABLE FULLY CHLORINATED GRAPHENE: CHLOROGRAPHENE

A. Structural Properties

In contrast to nonbonding chair conformation, our analysis indicates that like graphane (CH) and fluorographene (CF), the chair structure, where one chlorine atom is attached to each carbon atom of buckled graphene alternatingly from top and bottom sides can be a stable structure. The optimized atomic structure and the hexagonal lattice are shown in Fig. 6 (a). The present study predicts its total energy $E_T=22.24$ eV/per primitive cell and its cohesive energy $E_{coh}=1.68$ eV. In

TABLE I: Calculated values for graphene, and graphene derivatives, such as graphane CH, fluorographene CF and chlorographene CCl. These are lattice constant (a); C-C bond distance (d_{CC}); C-X bond distance (d_{CX}); thickness of the layer (t); photoelectric threshold (Φ); charge transfer from C to X ($\Delta\rho$); cohesive energy per unit cell (E_{coh}), formation energy (E_f), desorption energy of a single X atom from the CX surface (E_{des}); direct band gap (E_g); band gap corrected with GW $_o$, $E_g^{GW_o}$; in-plane stiffness (C); Raman active modes. Energies are calculated in (2x2) supercell.

Material (CX)	a Å	d_{CC} Å	d_{CX} Å	t Å	Φ eV	$\Delta\rho$ e	E_{coh} eV	E_f eV	E_{des}^X eV	E_g eV	$E_g^{GW_o}$ eV	C J/m ²	R-active Modes cm ⁻¹
Graphene	2.46	1.42	-	-	4.49	-	17.87	-	-	-	-	335	1600
CH	2.51	1.52	1.12	2.68	4.79	0.06	23.60	+0.39	4.79	3.42	5.97	243	1162, 1164, 1341, 2806
CF	2.55	1.55	1.37	3.22	7.93	-0.61	25.31	+2.04	5.46	2.96	7.49	250	245, 681, 1264, 1305
CCl	2.84	1.72	1.73	3.96	3.67	-0.13	19.60	-0.95	1.28	1.21	4.33	186	105, 398, 715, 1042

the rest of paper we name this stable structure as chlorographene or CCl, which should be distinguished from the unstable, nonbonding chair structure presented in the previous section in Fig. 5 (b). The remarkable situation is that the sp^2 -bonded planar graphene is buckled by $\delta=0.50$ Å, once it is converted to CCl. This way the local configuration of three folded sp^2 -bonding has changed to four folded sp^3 -bonding, reminiscent of tetrahedrally coordinated diamond structures. Formation of four folded sp^3 -bonding through buckling is essential for the stabilization of CCl, despite the C-C distance increased from 1.42 Å to 1.72 Å. On the other hand, while the C-Cl ionic bond in the adsorption of single Cl atom is 2.54 Å in Sec.III, it transforms to a covalent bond by contracting to 1.73 Å in chlorographene, which is also very close to the bond length of CCl₄ molecule. The bond length of chlorographene can also be contrasted with the Cl-graphene distance in nonbonding chair structure discussed in the previous section. We note that chlorographene is stable despite its cohesive energy is smaller than that of the unstable nonbonding chair conformation. This is due to the fact that chlorographene corresponds to a local minimum in Born-Oppenheimer surface.

In Table I we compare the structural parameters, relevant energies like cohesive energy, formation energy and desorption energy of graphene, CH, CF and CCl, all calculated by using LDA. It is seen that chlorographene, CCl has binding energy $E_b=1.68$ eV per unit cell relative to bare graphene and free Cl atom, and lowest E_{coh} (19.60 eV) per unit cell among other possible graphene derivatives. However, once CCl is synthesized a desorption energy of $E_{des}=1.28$ eV is required to take a single Cl atom out.

B. Vibrational Properties and Raman Spectra

Chlorographene (CCl) possesses D_{3d} point group symmetry. Phonon bands of CCl is shown in Fig. 6(b). It is seen that all the phonon modes have positive frequencies and hence the predicted structure of chlorographene is stable at T=0 K. Unlike the phonon bands of non-

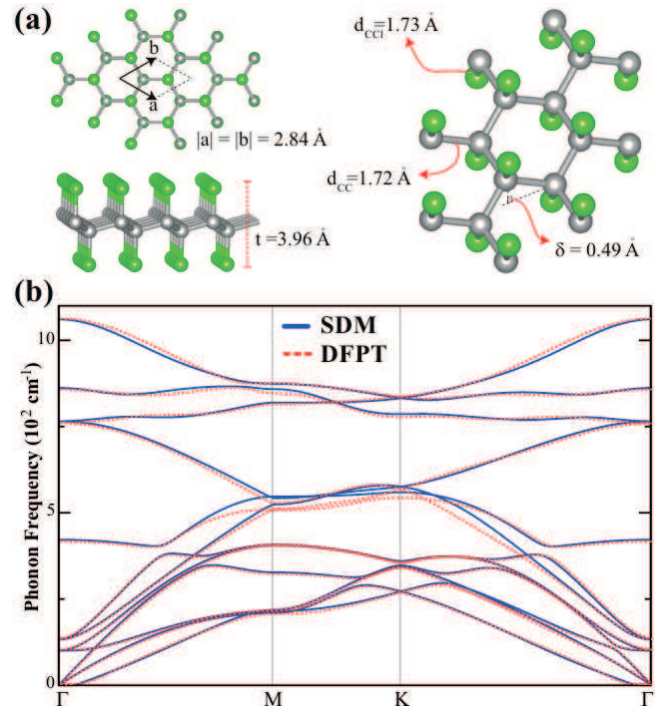


FIG. 6: (Color online) (a) Top, side and tilted views for the atomic structure of chlorographene CCl layer having hexagonal lattice and honeycomb structure. Carbon and chlorine atoms are indicated by gray (dark) and green (light) balls, respectively. Calculated structural parameters are indicated. (b) Phonon bands of chlorographene calculated using by SDM⁴³ and DFPT⁴⁴ methods.

bonding conformer, C-Cl bonds of chlorographene participate to all acoustic phonon branches. Therefore, the phonon spectrum of chlorographene differs from the spectrum of graphene. Though the chlorographene belongs to the same space group with CH and CF,^{22,23} the phonon frequencies are lowered (softened) due to the saturation of C atoms with heavy Cl atoms. While LA and TA modes have linearly dependent to phonon wave vector, ZA mode has a quadratic dispersion in the vicinity of Γ -

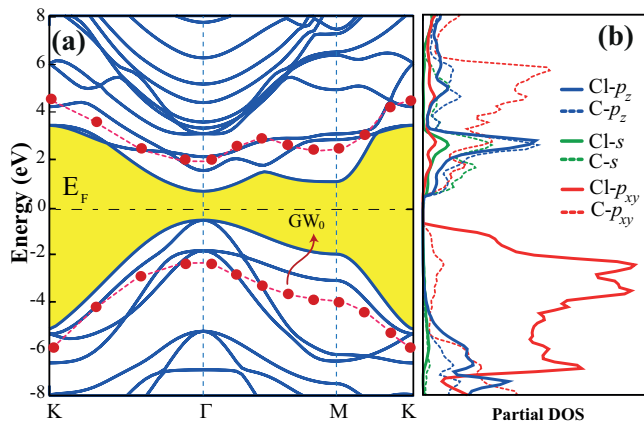


FIG. 7: (Color online) (a) Electronic band structure of chlorographene CCl. The band gap is shaded yellow. The GW_o corrected valance and conduction bands are shown by dashed line and red balls. The zero of energy set to the Fermi level E_F . (b) Density of states projected to various orbitals (PDOS).

point.^{22,23,52} As compared to single layer graphene, LO and TO (ZO) optical modes are softened from 1600 (900) to 1061 (421) cm^{-1} due the existence of surrounding Cl layers. In general, both phonon bands calculated using SDM and DFPT agree well, but they slightly differ at M and K point for optical phonon branches near at 500 cm^{-1} .

Group theory analysis shows that the decomposition of the vibration representation at the Γ -point is $\Gamma = 2A_{1g} + 2A_{2u} + 4E_g + 4E_u$. Among these, the modes at 105, 398, 715 and 1042 cm^{-1} are bond stretching modes and are Raman-active. Raman mode A_{1g} at 1042 (398) is entirely due to the out-of-plane vibration of C and Cl atoms moving in the same (opposite) direction with respect to each other. The observation of these Raman active modes are expected to shed light on the Cl coverage and the structure of chlorinated graphene. The observation of characteristic D-peak at 1330, G-peak at 1587 and 2D-peak at 2654 cm^{-1} from chlorinated graphene indicates low coverage of Cl.²⁶ Since the Raman measurements were performed in the range of 1250-3500 cm^{-1} , possible Raman-active peaks originating from chlorine atoms could not be observed.

C. Stability of CCl at finite temperature

Here we investigate whether CCl is stable at finite temperature, even though all phonon modes having positive frequencies in the Brillouin zone indicate its stability at $T=0$ K. This is achieved by carrying out ab-initio molecular dynamics (MD) calculations at finite temperatures using (6x6) supercell involving 144 C and one Cl atoms. Here we summarize our findings. At relatively low temperatures, for example at $T=500$ K, the perfect CCl remained stable even after ~ 6000 time steps of 2 fs. Even if 6000 time steps large for ab-initio calculations, but low

to attain a reliable statistics, this result suggests the stability of perfect CCl near room temperature. However, Cl atoms dissociate from CCl at 1000 K. This may be interpreted that CCl cannot be stable at elevated temperatures. Ab-initio MD calculations with single Cl vacancy at one side brought about the formation of a second vacancy at the other side after 200 time steps at 500 K. Thereafter, the structure continued to be stable. However, an island of Cl at both sides of graphene, for example, 6 Cl atoms adsorbed to a hexagon of graphene alternatingly from the top and bottom side of graphene is found unstable.

Our analysis using finite temperature ab-initio MD calculations led us to draw the following conclusion from the above results: A perfect CCl is stable at $T=0$ K and can remain stable possibly at room temperature. The creation of a single vacancy at one site imposes the formation of a second vacancy at the opposite side. This pair of vacancy can survive at room temperature. However, CCl having vacancies or holes is vulnerable to dissociation through the formation of Cl_2 molecules. The negative formation energy underlies these instabilities.

D. Electronic Properties

We present the band structure and the orbital decomposed density of states of fully chlorinated graphene CCl in Fig. 7. As a consequence of transition from sp^2 - to of sp^3 -type bonding and the mixing with Cl orbitals through Cl-C covalent bonds, linearly crossing semimetallic bands of graphene changes dramatically and turn to a nonmagnetic semiconductor with a direct band gap of $E_g = 1.21$ eV (GGA+vdW value: 1.55 eV) at the center of BZ. The two-fold degenerate bands at the top of valence band are mainly composed of the p_{xy} valence orbitals of Cl and C atoms and belong to the E_g irreducible representation. However, non-degenerate conduction band edge is formed by the hybridization of C- p_{xy} , C- p_z , C- s and Cl- p_z and belongs to the A_{2u} irreducible representation. Calculated values relevant for the electronic properties of CCl are given together with those of graphene, CH and CF in Table I. CCl has the lowest band gap (1.21 eV) among graphene derivatives, i.e. graphene ($E_g = 3.42$ eV) and fluorographene ($E_g = 2.96$ eV). Our calculations also reveals that the experimentally observed energy gap of 0.045 eV may arise from the partially chlorinated regions. Since DFT usually underestimates the band gaps, the band gap of 3D bulk crystals are successfully corrected by GW_o self-energy method. In the present paper we apply GW_o method to correct valance and conduction bands and hence the band gap of CCl. We found the corrected band gap 4.33 eV. This is a dramatic increase. Similar situation occurred for the correction of band gaps carried out for single layer structures, such as BN^{53} , CF^{23} and MoS_2^{54} . In particular, while LDA predicted band gap of single layer MoS_2 agrees with experiment, GW_o correction yielded very large band gap.

This situation led us to question whether GW_o correction is suitable for single layer structures.

While graphene have a positively charged surface due to the electron transferred from H to C atoms, Cl layers of CCl are negatively charged since 0.13 electrons (GGA+vdW value: 0.10 electrons) are transferred from C to Cl atoms. We also note that the effective charge is reduced from 0.42 to 0.13 electrons by going from ionic C-Cl bond in single Cl adsorption to the covalent C-Cl bond of chlorographene. Since CCl surfaces are negatively charged, it is possible to lower the photoelectric threshold of graphene from 4.49 eV to 3.67 eV by covering its surfaces with chlorine atoms. In contrast, as one notices in Table I, both fluorinated²³ and hydrogenated^{14,22} derivatives of graphene have photoelectric thresholds higher than graphene and CCl. The lower photoelectric threshold provide materials highly emissive surfaces. This facile photoemission feature is desirable for fast laser applications.^{55,56}

E. Mechanical Properties

Earlier studies have shown that graphene^{15,16} and fluorographene^{22,23} derivatives are strong materials like graphene. Among the three graphene derivatives chlorographene is the thickest one and we can expect some different mechanical properties. We will discuss the structural rigidity of chlorographene within the harmonic range of the elastic deformation, where the structure responded to strain ϵ linearly and reversibly. In the elastic range, in-plane stiffness C would be a good measure of the response of material. Here we use the expression to calculate in-plane stiffness, $C = (1/A_0) \cdot (d^2E_s/d\epsilon^2)$, where A_0 is the equilibrium area of the supercell and the strain energy is defined as the total energy at a given uniform strain minus the total energy at zero strain, namely $E_s = E_T(\epsilon) - E_T(\epsilon = 0)$. Here the strain in one direction is $\epsilon = \Delta c/c_0$, where c_0 is the equilibrium lattice constant of supercell and Δc is its stretching. For CCl we calculated C as 186 J/m^2 which identifies it as strong as CH and CF.

In Fig. 8(a) we show the variation of the strain energy E_s and its derivative with respect to the applied uniform strain, $dE_s/d\epsilon$. The latter is linear for small ϵ in the harmonic range. The elastic deformation occurs until the maximum of $dE_s/d\epsilon$, whereby the structure attains its initial state when the applied strain is lifted. Beyond the maximum the structural instabilities sets in with irreversible deformations. The region beyond the maximum is called plastic region. It seen that CCl undergoes instability, under 0.15 expansion of the lattice. Whereas, the critical expansion values are 0.20 and 0.24 for CF and CH, respectively.

We also calculated the effect of elastic strain on the band gap of CCl, CF and CH and presented our results in Fig. 8(b). CH and CCl have similar response to elastic strain: The increase of their band gaps for small strain is

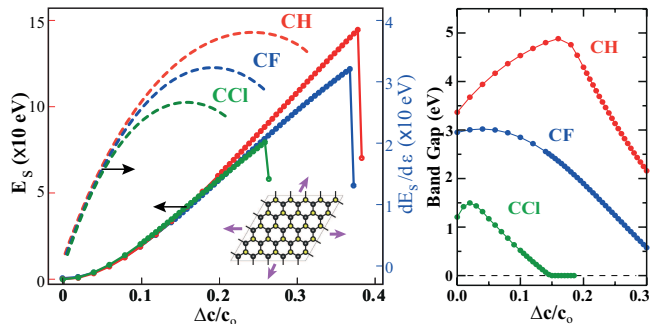


FIG. 8: (Color online) (a) The variation of the strain energy E_s (curves at the right hand side) and its derivative with respect to applied uniform strain ϵ , i.e. $dE_s/d\epsilon$, (curves at the left hand side) are calculated for CCl, CH and CF. After the maxima these structures become unstable and undergoes a plastic deformation. (b) Variation of the band gap with uniform strain. Calculations performed in (5×5) supercells.

followed by a rapid decrease for large strain. In contrast, initially the band gap of CF does not show any significant increase with increasing strain; for small strain it is almost unaltered, but decreases rapidly for large strain. Because of its smaller band gap, the metalization of CCl occurs earlier in the course of expansion.

VI. CONCLUSIONS

Motivated with the recent work by Li et al.²⁶, who achieved the photochemical chlorination of a bare graphene, we performed a first principle study on the chlorination of graphene starting from a single Cl adatom adsorption to fully chlorinated graphene CCl. We found that even if a Cl atom can be bound to graphene with a significant binding energy, it can migrate on the surface of graphene almost without an energy barrier. Formation of a Cl_2 molecule from two individual, migrating adatoms is energetically favorable when they are at close proximity. Therefore the formation energy of the adsorption of a single Cl atom relative to Cl_2 molecule is negative. In this respect, all possible configurations or decoration obtained by the chlorination of one surface of graphene and considered in this study are not stable. On the other hand, the configuration, where two Cl atoms are adsorbed from opposite sides of graphene to two adjacent carbon atoms forming sp^3 -type covalent C-Cl bonds and hence inducing buckling are stable, since the dissociation of these two Cl atoms by forming Cl_2 molecule is hindered. Once the bare graphene is fully chlorinated from both side inducing buckling of carbon atoms, the resulting conformation named as chlorographene, is stable at T=0 K and also possibly at room temperature. With its 1.21 eV direct band gap, stiff mechanical properties and response to homogeneous strain this material displays interesting properties for future technological applications. On the other hand, the nonbonding chair conformation has cohesive

energy higher than that of chlorographene in the chair conformation and is found to be unstable. While both structures are not in ground state, chlorographene corresponds to a local minimum on the Born-Oppenheimer surface. Of course, a state having the energy lower than those of both conformation is Cl_2 molecules, which are weakly attached to bare graphene.

VII. ACKNOWLEDGEMENTS

The authors thank Dr M. Topsakal for his assistance regarding the stability of chlorographene and Mr

O. Ozcelik for his assistance in specific calculations. This work is supported by TUBITAK through Grant No:108T234. Part of the computational resources has been provided by TUBITAK ULAKBIM, High Performance and Grid Computing Center (TR-Grid e-Infrastructure). S. C. acknowledges the partial support of TUBA, Academy of Science of Turkey.

-
- * New address: Departement Fysica, Universiteit Antwerpen, Groenenborgerlaan 171, B-2020 Antwerpen, Belgium
- † Corresponding author: ciraci@fen.bilkent.edu.tr
- ¹ Novoselov, K.; Geim, A.; Morozov, S.; Jiang, D.; Zhang, Y.; Dubonos, S.; Grigorieva, I.; Firsov, A. *Science* **2004**, 306, 666-669
 - ² Novoselov, K. S.; Geim, A. K.; Morozov, S. V.; Jiang, D.; Katsnelson, M. I.; Grigorieva, I. V.; Dubonos, S. V.; Firsov, A. A. *Nature* **2005**, 438, 197-200
 - ³ Geim, A. K.; Novoselov, K. S. *Nat. Mater.* **2007**, 6, 183-191
 - ⁴ Geim, A. K. *Science* **2009**, 324, 1530-1534
 - ⁵ Katsnelson, M. I.; Novoselov, K. S.; Geim, A. K.; *Nat. Phys.* **2006**, 2, 620-625.
 - ⁶ Dikin, D. A.; Stankovich, S.; Zimney, E. J.; Piner, R.; Dommett, G. H. B.; Evmenenko, G.; Nguyen, S. T.; Ruoff, R. S. *Nature* **2007**, 448, 457-460.
 - ⁷ Eda, G.; Fanchini G.; Chhowalla, M.; *Nature Nanotech.* **2008**, 3 270-274.
 - ⁸ Gomez-Navarro, C.; Weitz, R. T.; Bittner, A. M.; Scolari, M.; Mews, A.; Burghard, M.; Kern, K.; *Nano Lett.* **2007**, 7, 3499-3503
 - ⁹ Gilje, S.; Han, S.; Wang, M.; Wang, K. L.; Kaner, R. B.; *Nano Lett.* **2007**, 7, 3394-3398
 - ¹⁰ Robinson, J. T.; Perkins, F. K.; Snow, E. S.; Wei, Z.; Sheehan, P. E.; *Lett.* **2008**, 8, 3137-3140
 - ¹¹ Kim, S.; Zhou, S.; Hu, Y.; Acik, M.; Chabal, Y. J.; Berger, C.; de Heer W.; Bongiorno, A.; Riedo, E.; *Nature Materials* **2012**, 11, 544-549
 - ¹² Elias, D. C.; Nair, R. R.; Mohiuddin, T. M. G.; Morozov, S. V.; Blake, P.; Halsall, M. P.; Ferrari, A. C.; Boukhvalov, D. W.; Katsnelson, M. I.; Geim, A. K.; Novoselov, K. S. *Science* **2009**, 323, 610.
 - ¹³ Flores, M. Z. S.; Autreto, P. A. S.; Legoas, S. B.; Galvao, D. S.; *Nanotechnology* **2009** 20, 465704-465706.
 - ¹⁴ Sahin, H.; Ataca, C.; Ciraci, C.; *Appl. Phys. Lett.* **2009**, 95, 222510.
 - ¹⁵ Sahin, H.; Ataca, C.; Ciraci, C.; *Phys. Rev. B* **2010**, 81, 205417; Sahin, H.; Ciraci, C.; *Phys. Rev. B* **2011**, 84, 035452.
 - ¹⁶ Topsakal, M.; Cahangirov, S.; Ciraci, S.; *Appl. Phys. Lett.* **2010**, 96, 091912.
 - ¹⁷ Sofo, J. O.; Chaudhari, A. S.; Barber, G. D.; *Phys. Rev. B* **2007**, 75 153401.
 - ¹⁸ Nair, R. R.; Ren, W.; Jalil, R.; Riaz, I.; Kravets, V. G.; Britnell, L.; Blake, P.; Schedin, F.; Mayorov, A. S.; Yuan, S.; Katsnelson, M. I.; Cheng, H.-M.; Strupinski, W.; Bulusheva, L. G.; Okotrub, A. V.; Grigorieva, I. V.; Grigorenko, A. N.; Novoselov, K. S.; Geim, A. K. *Small* **2010**, 6, 2877.
 - ¹⁹ Cheng, S. -H.; Zou, K.; Okino, F.; Gutierrez, H. R.; Gupta, A.; Shen, N.; Eklund, P. C.; Sofo, J. O.; Zhu, J.; *Phys. Rev. B* **2010**, 81 205435.
 - ²⁰ Robinson, J. T.; Burgess, J. S.; Junkermeier, C. E.; Badescu, S. C.; Reinecke, T. L.; Perkins, F. K.; Zalalutdniov, M. K.; Baldwin, J. W.; Culbertson, J. C.; Sheehan, P. E.; Snow, E. S. *Nano Lett.* **2010**, 10, 3001-3005
 - ²¹ Withers, F.; Dubois, M.; Savchenko, A. K.; *Phys. Rev. B* **2010**, 82 073403.
 - ²² Peelaers, H.; Hernandez-Nieves, A. D.; Leenaerts, O.; Partoens, B.; Peeters, F. M.; *Appl. Phys. Lett.* **2011**, 98 051914.
 - ²³ Sahin, H.; Topsakal, M.; Ciraci, S., *Phys. Rev. B* **2011**, 83 115432.
 - ²⁴ Charlier, J.-C.; Gonze, X.; Michenaud, J. -P.; *Phys. Rev. B* **1993**, 47 16152.
 - ²⁵ Takagi, Y.; Kusakabe, K.; *Phys. Rev. B*, **2002**, 65 121103.
 - ²⁶ Li, B.; Zhou, L.; Wu, D.; Peng, H.; Yan, K.; Zhou, Y.; Liu, Z. F. *ACS NANO* **2011**, 5, 5957-5961
 - ²⁷ Wu, J.; Xie, L.; Li, Y.; Wang, H.; Ouyang, Y.; Guo, J.; Dai, H.; *J. Am. Chem. Soc.* **2011** 133 19668
 - ²⁸ Gopalakrishnan, K.; Subrahmanyam, K. S.; Kumar, P.; Govindaraj, A.; Rao, C. N. R.; *RSC Adv.*, **2012** 2 1605.
 - ²⁹ Wehling, T. O.; Katsnelson, M. I.; Lichtenstein, A. I.; *Phys. Rev. B* **2009**, 80 085428.
 - ³⁰ Klintenberg, M.; Lebegue, S.; Katsnelson, M. I.; Eriksson, O.; *Phys. Rev. B* **2010**, 81 085433.
 - ³¹ Medeiros, P. V. C.; Mascarenhas, A. J. S.; Mota, F. D.; de Castilho, C. M. C. *Nanotechnology* **2010**, 21, 485701
 - ³² Zboril, R.; Karlicky, F.; Bourlino, A. B.; Steriotis, T. A.; Stubos, A. K.; Georgakilas, V.; Safarova, K.; Jancik, D.; Trapalis, C.; Otyepka, M. *Small* 2010, 6, 2885-2891
 - ³³ Rudenko, A. N.; Keil, F. J.; Katsnelson, M. I.; Lichtenstein, A. I.; *Phys. Rev. B* **210**, 82 035427.
 - ³⁴ Dhiman, P.; Yavari F.; Mi, X.; Gullapalli, H.; Shi, Y.; Ajayan, P.M.; Koratkar, N.; *Nano Lett.* **2011**, 11, 3123-3127
 - ³⁵ Ijäs, M.; Havu, P.; Harju, A.; *Phys. Rev. B* **2012**, 85 035440.
 - ³⁶ Yang, M.; Zhou, L.; Wang, J.; Liu Z.; Liu, Z.; *J. Phys.*

- Chem. C, **2012**, 116, 844.
- ³⁷ Blochl, P. Phys. Rev. B **1994**, 50, 17953-17979
- ³⁸ Ceperley, D.; Alder, B. Phys. Rev. Lett. **1980**, 45, 566-569
- ³⁹ Perdew, J. P.; Burke, K.; Ernzerhof, M. Phys. Rev. Lett. **1996**, 77, 3865-3868
- ⁴⁰ Grimme, S. J. Comput. Chem. **2006**, 27, 1787-1799.
- ⁴¹ Kresse, G.; Furthmuller, J. Phys. Rev. B **1996**, 54, 11169-11186
- ⁴² Henkelman, G.; Arnaldsson, A.; Jonsson, H. Comput. Mater. Sci. **2006**, 36, 354-360
- ⁴³ Alfe, D. Comput. Phys. Commun. **2009**, 180, 2622-2633
- ⁴⁴ Giannozzi, P.; Baroni, S.; Bonini, N.; Calandra, M.; Car, R.; Cavazzoni, C.; Ceresoli, D.; Chiarotti, G. L.; Cococcioni, M.; Dabo, I.; Corso, A. D.; Gironcoli, S.; Fabris, S.; Fratesi, G.; Gebauer, R.; Gerstmann, U.; Gougoussis, C.; Kokalj, A.; Lazzeri, M.; Martin-Samos, L.; Marzari, N.; Mauri, F.; Mazzarello, R.; Paolini, S.; Pasquarello, A.; Paulatto, L.; Sbraccia, C.; Scandolo, S.; Sclauzero, S.; Seitsonen, A. P.; Smogunov, A.; Umari, P.; Wentzcovitch, R. M. J. Phys. Condens. Matter **2009**, 21, 395502
- ⁴⁵ Shishkin, M.; Kresse, G. Phys. Rev. B **2006**, 74, 035101
- ⁴⁶ The total energy of magnetic states or non-magnetic states, whichever is lower, are used in calculating binding, cohesive and formation energies.
- ⁴⁷ Heyd, J.; Scuseria, G.; Ernzerhof, M. J. Chem. Phys. **2003**, 118, 8207-8215
- ⁴⁸ The experimental value for the binding energy of Cl₂ molecule is 2.52 eV (Haynes, W. M.; Lide, D. R. CRC handbook of chemistry and physics, 91st ed.; CRC: London, 2010, p. 57.). We also calculated the binding energy of Cl₂ using PBE and GGA+vdW to be 3.08 eV and 3.02 eV, respectively. By applying corrections within hybrid functionals (see Ref 45) and performing LDA+HSE06, PBE+HSE06 and GGA+HSE06 calculations the binding energies of Cl₂ is found to be 3.10 eV, 2.65 eV and 2.60 eV. The latter value calculated with GGA+HSE06 is in excellent agreement with the experimental value. Earlier calculations reported the binding energies of Cl₂ to be 3.78 eV [Liu, Z. F.; Chan, S.P. Chem. Phys. Lett. **2000**, 318, 15-21], 2.68 eV [Gao, W.; Baker, T. A.; Zhou, L.; Pinnaduwaage, D. S.; Kaxiras, E.; Friend, C. M. J. Am. Chem. Soc. **2008**, 130, 3560-3565] and 2.54 eV [Broqvist P.; Molina, L. M.; Gronbeck H.; Hammer B. J. Catal. **2004**, 227, 217-226]. The LDA method with PAW potential used in the present paper yields overbinding. Since LDA method is used consistently throughout the paper the overbinding did not affected our conclusions.
- ⁴⁹ Kittel, C. Introduction to Solid State Physics, 7th ed.; Wiley: New York, **1996**.
- ⁵⁰ Chan, K. T.; Neaton, J. B.; Cohen, M. L.; Phys. Rev. B **2008**, 77, 235430.
- ⁵¹ Sahin, H.; Cahangirov, S.; Topsakal, M.; Bekaroglu, E.; Akturk, E.; Senger, R. T.; Ciraci, S. Phys. Rev. B **2009**, 80, 155453
- ⁵² Yan, J. -A.; Ruan, W. Y.; Chou, M. Y.; Phys. Rev. B **2008**, 77 125401.
- ⁵³ Topsakal, M.; Akturk, E.; Ciraci, S.; Phys. Rev. B **2009**, 79 115442.
- ⁵⁴ Ataca, C.; Sahin, H.; Akturk, E.; Ciraci, S. J. Phys. Chem. C **2011**, 115, 3934-3941
- ⁵⁵ Allen, F. G.; Gobeli, G. W.; Phys. Rev. **1962**, 127 150.
- ⁵⁶ Ditchfield, R; Llera-Rodriguez, D.; Seebauer, E. G.; Phys. Rev. B **2000**, 61 13 710.